Direct Measurement of the Radial Electric Field in Tokamak Plasmas using the Stark Effect

B. W. Rice,* K. H. Burrell, L. L. Lao, and Y. R. Lin-Liu
General Atomics, P.O. Box 85608, San Diego, California 92186–5608
(Received 17 June 1997)

Motional Stark effect polarimetry (MSE) is a well established technique for measuring the magnetic field pitch angle in tokamaks. By viewing the Stark emission spectrum from two different angles, this technique can also provide local measurements of the plasma radial electric field, E_r. Simultaneous measurements of the profiles of magnetic field pitch angle and E_r are presented for the first time in a high-performance DIII-D tokamak plasma. Direct measurement of E_r is of great importance in fusion research because the suppression of turbulence through $\mathbf{E}_r \times \mathbf{B}$ velocity shear provides a mechanism to improve energy confinement. [S0031-9007(97)04195-1]

PACS numbers: 52.70.Kz, 52.55.Fa

One of the recent success stories in tokamak physics has been the development of improved confinement regimes, accessed through shaping of the magnetic field pitch or safety factor profile. The safety factor, q, is defined as the rate of change of toroidal flux with poloidal flux; magnetic shear is defined as $s \equiv (2V/q)(dq/dV)$ where V is the flux surface volume. In discharges with negative central magnetic shear (NCS), where the q profile has an off-axis minimum, improvements in core confinement have been observed. With neutral beam heating, central ion thermal transport—and in some cases particle transport—approaches neoclassical levels [1–4]. Under some conditions, reductions in central electron thermal transport is also observed [4,5]. The NCS q profile is also advantageous for magnetohydrodynamic (MHD) stability of the plasma, providing stability to $n/m = 1/1$ sawteeth and kink modes, and high-n ballooning modes in the core. Record levels of fusion gain have been achieved on the DIII-D [6] and JT-60U [7] in this regime. Progress in this area has largely been due to the development of diagnostic techniques such as the motional Stark effect (MSE) to measure the q profile reliably and quickly in between plasma discharges. MSE was first demonstrated on PBX-M [8], and is now used routinely on DIII-D [9–11] and many other tokamaks.

Low levels of ion thermal transport and reduced turbulence have also been observed in discharges with monotonic q profiles such as the *VH* mode on DIII-D [12], supershots on TFTR [13], and the high β_p mode on JT-60U [14]. Although strong negative shear does not exist in these discharges, they generally are free from sawtooth oscillations. While the shape of the q profile is important for macroscopic stability to ideal and resistive MHD modes, the reduction in small-scale microturbulence observed in these different regimes is not easily explained through the q profile shape alone. The most successful model to date for explaining the improvement in transport observed in many of these regimes is based on $\mathbf{E}_r \times \mathbf{B}$ velocity shear stabilization of turbulence in the plasma [15], where E_r is the plasma radial electric field. This model was originally developed to explain the *H* mode edge transport barrier [15]. The basic idea is that $\mathbf{E}_r \times \mathbf{B}$ velocity shear can reduce both the growth rate and radial extent of turbulent eddies in the plasma, thus reducing thermal transport. This model has been tested on many tokamaks now, and generally seems to be in agreement with experiments, although additional quantitative testing is necessary.

The presence of E_r in tokamaks is simply the result of radial force balance in the plasma given by

$$E_r = (Z_i e n_i)^{-1} \nabla P_i - v_{\theta i} B_\phi + v_{\phi i} B_\theta , \qquad (1)$$

where Z_i is the ion charge, n_i is the ion density, e is the electronic charge, P_i is the ion pressure, $v_{\theta i}$, $v_{\phi i}$ are the poloidal and toroidal fluid rotation velocities, respectively, and B_θ, B_ϕ are poloidal and toroidal fields. This equation is valid for both the main ion and impurity species. The direction of E_r is perpendicular to the flux surface. On DIII-D, with strong tangential neutral beam injection, the formation of E_r in the core is generally dominated by toroidal flow; the ∇P_i and v_θ terms are also significant at the edge. If, through a combination of increased beam power and optimizing the q profile, the $\mathbf{E}_r \times \mathbf{B}$ velocity shearing rate can be increased above the threshold for turbulence suppression, then confinement improves, resulting in larger rotation velocities and E_r, thus establishing a positive feedback mechanism [15].

It was recognized recently that the large values of E_r observed in all high-performance plasmas—up to 200 kV/m in DIII-D—can significantly affect the interpretation of MSE measurements of the q profile [16,17]. It was also shown that with additional MSE measurements, one can extract a direct measurement of E_r in addition to the usual magnetic field pitch measurement. During a recent vent on DIII-D, 19 additional MSE channels with new viewing angles were added to the existing system [10,11] (for a total of 35 channels) in order to resolve the E_r field. In this Letter, the system upgrade will be described, and the first measurements demonstrating simultaneous measurement of the q and E_r profiles in high-performance plasmas will be presented. We show that the E_r effect does indeed change our

 0031-9007/97/79(14)/2694(4)$10.00

interpretation of the q profile and that the direct MSE measurement of E_r is in good agreement with the value calculated from charge-exchange recombination measurements of the terms on the right-hand side of Eq. (1). This reliable and fast (available between discharges) measurement of these two important quantities which affect plasma stability and confinement provides fusion researchers an important new tool for advancing the understanding and optimization of tokamak plasmas.

The MSE measurement relies upon the splitting of the Balmer-α line into orthogonally polarized components (σ, π) as a result of the strong electric field in the rest frame of deuterium atoms injected by a high-energy neutral beam. When viewed in a direction perpendicular to $\mathbf{E}$, the Stark components σ and π are polarized perpendicular and parallel to $\mathbf{E}$, respectively. The total electric field in the rest frame of the neutral beam atoms traveling with velocity v_b is the sum of the Lorentz $\mathbf{E}_b = \mathbf{v}_b \times \mathbf{B}$ field and the plasma radial electric field given by Eq. (1). The relationship between the polarization angle of the Stark σ component and the magnetic field and E_r components has been derived previously [16]. Using the viewing geometry shown in Fig. 1, the polarization angle of the electric field is given by

$$\tan\gamma = \frac{A_1 B_z + A_5 E_R}{A_2 B_\phi + A_3 B_R + A_4 B_Z + A_6 E_Z + A_7 E_R}, \tag{2}$$

where R is the major radius and Z is in the vertical direction. The A coefficients are viewing geometry dependent terms given by

$$\begin{aligned} A_1 &= -\cos(\alpha + \Omega), \\ A_2 &= \sin\alpha\cos\theta, \\ A_3 &= \cos\alpha\cos\theta, \\ A_4 &= \sin(\alpha + \Omega)\sin\theta, \\ A_5 &= -\cos(\Omega)/v_b, \\ A_6 &= -\cos\theta/v_b, \\ A_7 &= \sin\theta\sin\Omega/v_b. \end{aligned}$$

On DIII-D, the quantities B_R, E_Z, and θ are small near the midplane giving the approximate relation

$$\tan\gamma \approx \frac{A_1 B_z + A_5 E_R}{A_2 B_\phi}. \tag{3}$$

In past analysis of MSE data, we assumed that the E_R component in Eq. (3) could be neglected. However, in recent high-performance plasmas, the E_R term in the numerator of Eq. (3) can be up to 25% of the B_Z term and therefore must be included in the analysis. Since coefficients A_1 and A_5 vary differently depending on viewing geometry and beam velocity, we see that with two MSE systems viewing the same radial location in the plasma but with different A_i coefficients, then both the poloidal field (B_Z) and the E_R field can be determined. To obtain this measurement on DIII-D, nineteen additional channels were added as indicated by the dashed lines of sight in Fig. 1, providing two different viewing angles for each location in the plasma. Because of the finite beam width of 14 cm, the new radial channels have worse spatial resolution ($\delta R \sim 13$–23 cm) than the tangential channels ($\delta R \sim 1.5$–5 cm). The hardware design for the new channels essentially duplicates that of the original system [11]. All chords are tuned to the full-energy component of the neutral beam. For the radial viewing channels, the coefficient A_5 is approximately zero, while for the tangential viewing chords $A_5 \approx 1/v_b$. Defining an effective measured vertical field as $B_{Z0} = (A_2/A_1)B_\phi \tan\gamma$ (i.e., the measured vertical field assuming $E_R = 0$), then the radial electric field at a radius R is given by

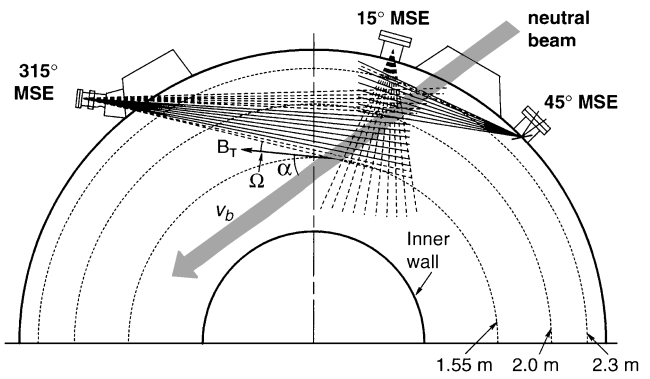

FIG. 1. Viewing geometry for 35 channel MSE system on DIII-D. The dashed lines indicate the line of sight for the new channels added to resolve E_r. There is a small tilt of the viewing lines out of the horizontal plane given by the angle θ.

$$E_R \approx \frac{A_1 A_1' (B_{Z0} - B_{Z0}')}{A_5 A_1' - A_1 A_5'}, \tag{4}$$

where the prime refers to the second view at a given radial location.

The simultaneous measurement of the q profile and E_r profile has been tested using a recent high-triangularity discharge obtained during commissioning of the new upper divertor hardware in DIII-D. The time evolution of several key parameters is given in Fig. 2. The plasma fuel is deuterium with a plasma current of 1.6 MA and toroidal field of 2.1 T. This discharge has confinement enhancement relative to the ITER89P scaling of $H = 3.5$ and normalized beta of $\beta_N = 3.6$ (% T m/MA) similar to VH mode or NCS plasmas, even though the edge localized mode (ELM)-free period is relatively short. In Fig. 2(c), the effective vertical field B_{Z0} (assuming $E_r = 0$) is plotted for a tangential chord (solid line) and a radial chord (dashed line) at a radius of $R = 2$ m. If E_r were zero, then these two curves would track one another. The separation of the two curves during the ELM-free period from 2–2.25 s is an indication of the buildup of radial

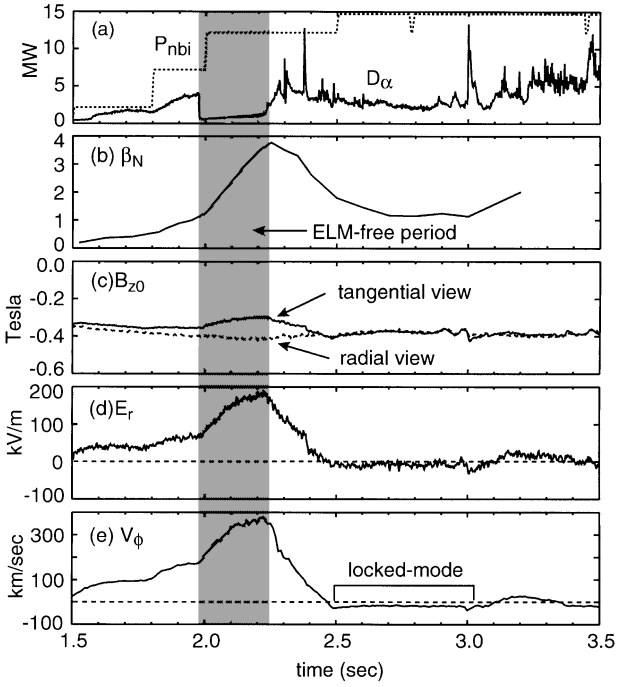

FIG. 2. Time evolution of discharge 92043: (a) neutral beam power and D_α emission, (b) normalized beta, (c) MSE B_{Z0} measurement at $R = 2$ m, (d) local value of E_r calculated from the data in (c) using Eq. (4), and (e) CER toroidal rotation at $R = 1.9$ m.

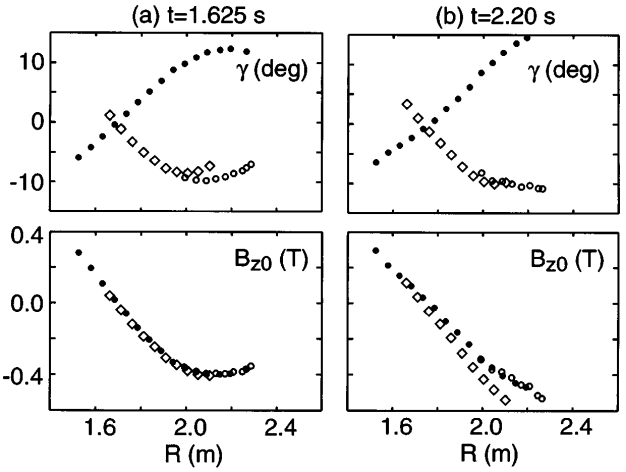

FIG. 3. Profiles of MSE pitch angle γ and B_{Z0} measurements for two phases of discharge 92043: (a) Low-power L-mode phase with low plasma rotation and E_r field; (b) high-performance phase with peak $E_r \sim 170$ kV/m. Circles are tangential chords and diamonds are radial chords.

electric field. Using Eq. (4), the radial electric field at $R = 2$ m is calculated directly from the MSE measurements as shown in Fig. 2(d). The time evolution of E_r follows closely the time evolution of the plasma toroidal rotation in Fig. 2(e) obtained from charge-exchange recombination (CER) [18] measurements of carbon impurities. The maximum time response of the MSE E_r measurement is 1 ms with an RMS noise resolution of 7 kV/m. The curve in Fig. 2(c) was generated using a 5 ms sliding boxcar average giving somewhat better resolution. Systematic errors in E_r due to spatial averaging in the radial chords and calibration are a factor of 2–3 larger than uncertainties due to noise at present. An additional point of interest in this discharge is that a locked mode develops after the collapse in β from 2.5–3 s. During this time the impurity rotation shows a small negative rotation. In agreement with this observation, the MSE radial electric field measurement also reverses sign during mode locking.

To determine the profile of E_r, we start by examining the profiles of pitch angle and B_{Z0} shown in Fig. 3. At 1.625 s, during the low-power L-mode portion of the discharge, the effective vertical field calculated from both the tangential (circles) and radial (diamonds) systems agree, indicating almost unmeasurable levels of E_r. However, by 2.2 s the tangential and radial profiles have significantly deviated from one another indicating large E_r.

The profiles of E_r and q can be determined from these data using the EFIT equilibrium reconstruction code [19]. EFIT is needed—especially in shaped plasmas—to map MSE measurements onto a flux surface geometry, and self-consistently solve for the E_r and magnetic field profiles that best match the measurements. Since E_r is not constant on a flux surface, EFIT instead fits to the gradient of the electrostatic potential Φ. Assuming Φ is constant on a flux surface then we have

$$\mathbf{E}_r = -\nabla\Phi = -\frac{\partial\Phi}{\partial\psi}\nabla\psi \tag{5}$$

$$= -\omega R B_R \hat{Z} + \omega R B_Z \hat{R}\,, \tag{6}$$

where ψ is the poloidal flux and we have introduced the definition $\omega \equiv \partial\Phi/\partial\psi$, which has dimensions of frequency. Either a polynomial or spline representation can be used for $\omega(\psi)$. EFIT uses Eq. (5) to calculate the components of E_R and E_Z for use in calculating the MSE pitch angle from Eq. (2). Then the fitting parameters for ω are adjusted simultaneously with parameters for the usual equilibrium functions p' and ff' [19] to minimize χ^2 on external magnetics, MSE measurements, and optionally pressure profile data.

Figure 4 shows the equilibrium reconstruction using a two term polynomial fit to ω for the MSE profile data in Fig. 3 at 2.2 s. In Fig. 4(a), the B_Z profile data is calculated including the E_R, E_Z terms, now showing good agreement between the tangential and radial views. The resulting q and E_r profiles are shown as the solid curves in Figs. 4(c) and 4(d), respectively. For comparison, the CER measurement of E_r obtained from Eq. (1) is also shown as the dashed line. The agreement between the two instruments is better than 20 kV/m over the entire plasma radius. Since E_r is a relatively smooth function in this case, no improvement in χ^2 was obtained by adding additional polynomial terms to the ω function. However, in other discharges with more structure in E_r, fitting functions with more degrees of freedom are necessary.

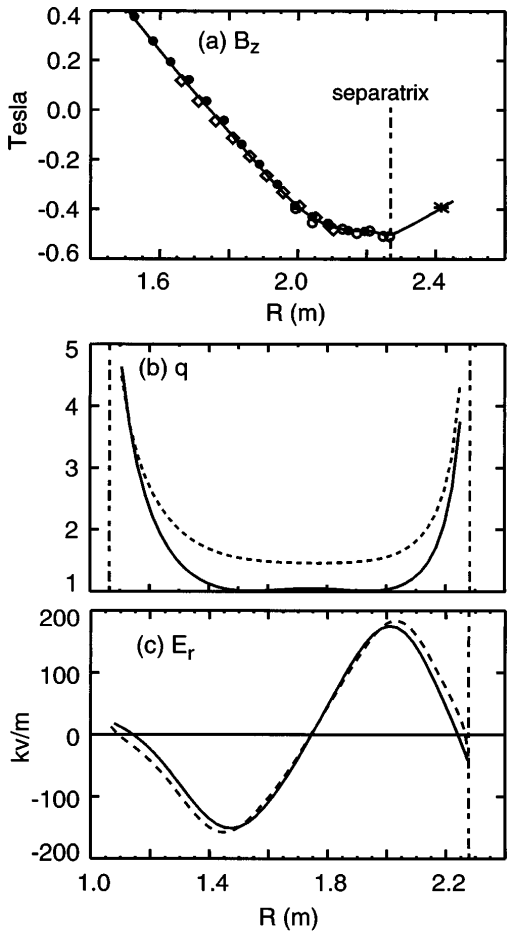

FIG. 4. EFIT equilibrium reconstruction including E_r for 92043 at 2.2 s: (a) MSE B_z data; (b) q profile obtained using all MSE chords and including E_r (solid line) versus that obtained using only tangential MSE chords and assuming $E_r = 0$ (dashed line); (c) E_r determined from EFIT (solid line) and CER analysis of carbon impurities (dashed line).

In addition to providing a direct local measurement of E_r, the new MSE measurements also allow the q profile to be calculated with improved accuracy. The dashed curve in Fig. 4(b) shows the q profile that results when only the tangential MSE chords are used and E_r is assumed to be zero. In Fig. 5, the time evolution of q_0 is shown calculated from EFIT using the tangential chords only and no E_r (dashed line) versus that calculated using all MSE chords including the E_r effect (solid line). The difference in q_0 is quite large, especially during the high-performance ELM-free period. Such changes would have an important effect on stability calculations.

In conclusion, it has been demonstrated on DIII-D that the MSE diagnostic can provide simultaneous measurements of the q and E_r profiles. The uncertainty in E_r due to noise is 7 kV/m or less depending on averaging. Possible systematic errors due to spatial averaging or offset calibration are currently about 2–3 times this level. The agreement with the E_r profile calculated independently from CER measurements is within experimental uncertainties. While EFIT reconstructions are required to give self-consistent solutions to both the E_r and q profile, a real-time measurement of local E_r suitable for feedback control of the $\mathbf{E}_r \times \mathbf{B}$ velocity shear can be obtained from the raw MSE data using Eq. (4). Given the importance of the effect of E_r and q profiles on plasma confinement and stability, this powerful measurement should continue to guide experiments in achieving improved fusion performance in tokamaks.

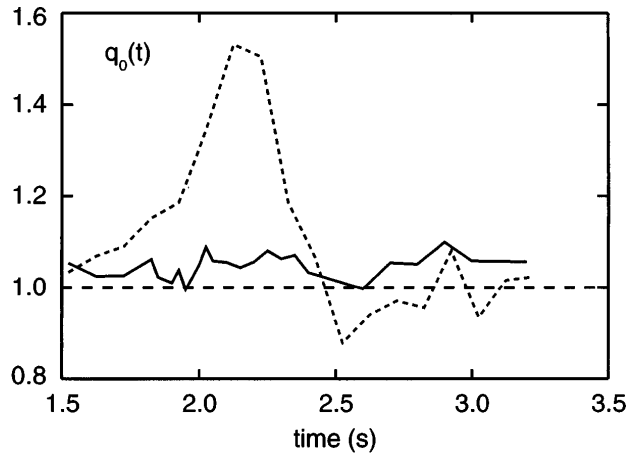

FIG. 5. Time evolution of q_0 determined by EFIT using full MSE system including E_r (solid line) versus using only the tangential channels and no E_r (dashed line).

This is a report of work supported by the U.S. Department of Energy under Contracts No. W-7405-ENG-48 and No. DE-AC03-88ER51114. The authors acknowledge the engineering support of D. G. Nilson in designing and fabricating the new chords.

*Visiting scientist from Lawrence Livermore National Laboratory, Livermore, CA 94551.

[1] E. J. Strait *et al.*, Phys. Rev. Lett. **75**, 4421 (1995).
[2] F. M. Levinton *et al.*, Phys. Rev. Lett. **75**, 4417 (1995).
[3] B. W. Rice *et al.*, Phys. Plasmas **3**, 1983 (1996).
[4] T. Fujita *et al.*, Phys. Rev. Lett. **78**, 2377 (1997).
[5] G. T. Hoang *et al.*, Nucl. Fusion **34**, 75 (1994).
[6] E. A. Lazarus *et al.*, Phys. Rev. Lett. **77**, 2714 (1996).
[7] Y. Koide *et al.*, Phys. Plasmas **4**, 1623 (1997).
[8] F. M. Levinton *et al.*, Phys. Rev. Lett. **63**, 2060 (1989).
[9] D. Wroblewski *et al.*, Rev. Sci. Instrum. **61**, 3552 (1990).
[10] D. Wroblewski and L. L. Lao, Rev. Sci. Instrum. **63**, 5140 (1992).
[11] B. W. Rice, D. G. Nilson, and D. Wroblewski, Rev. Sci. Instrum. **66**, 373 (1995).
[12] G. L. Jackson *et al.*, Phys. Rev. Lett. **67**, 3098 (1991).
[13] J. Strachan *et al.*, Phys. Rev. Lett. **58**, 1004 (1987).
[14] T. Nishitani *et al.*, Nucl. Fusion **34**, 1069 (1994).
[15] K. H. Burrell, Phys. Plasmas **4**, 1499 (1997).
[16] B. W. Rice *et al.*, Nucl. Fusion **37**, 517 (1997).
[17] M. C. Zarnstorff *et al.*, Phys. Plasmas **4**, 1097 (1997).
[18] P. Gohil *et al.*, in *Proceedings of the 14th IEEE/NPSS Symposium on Fusion Technology* (IEEE, NY, 1992), Vol. II, p. 1199.
[19] L. L. Lao *et al.*, Nucl. Fusion **30**, 1035 (1990).